

# The H I opacity of the intergalactic medium at redshifts $1.6 < z < 3.2$

David Kirkman\* †, David Tytler† Nao Suzuki†, Carl Melis, Susan Hollywood, Kory James, Geoffrey So, Dan Lubin† Tridivesh Jena, Michael L. Norman, and Pascal Paschos

*Center for Astrophysics and Space Sciences, University of California San Diego, La Jolla, CA, 92093-0424*

27 June 2018

## ABSTRACT

We use high quality echelle spectra of 24 QSOs to provide a calibrated measurement of the total amount of Ly $\alpha$  forest absorption (DA) over the redshift range  $2.2 < z < 3.2$ . Our measurement of DA excludes absorption from metal lines or the Ly $\alpha$  lines of Lyman limit systems and damped Ly $\alpha$  systems. We use artificial spectra with realistic flux calibration errors to show that we are able to place continuum levels that are accurate to better than 1%. When we combine our results with our previous results between  $1.6 < z < 2.2$ , we find that the redshift evolution of DA is well described over  $1.6 < z < 3.2$  as  $A(1+z)^\gamma$ , where  $A = 0.0062$  and  $\gamma = 2.75$ . We detect no significant deviations from a smooth power law evolution over the redshift range studied. We find less H I absorption than expected at  $z = 3$ , implying that the UV background is about 40% higher than expected. Our data appears to be consistent with an H I ionization rate of  $\Gamma \sim 1.4 \times 10^{-12} \text{ s}^{-1}$ .

**Key words:** quasars: absorption lines – cosmology: observations – intergalactic medium.

## 1 INTRODUCTION

The mean optical depth of the H I Ly $\alpha$  forest observed in the spectra of high redshift QSOs is one of the main pieces of information on the physical state of the intergalactic medium (IGM). This is because the optical depth of the Ly $\alpha$  forest ( $\tau_{\text{eff}}$ ) is sensitive to the combination of a wide variety of effects that we can collect under two main headings (Rauch et al. 1997). First,  $\tau_{\text{eff}}$  is sensitive to all the familiar parameters of the cosmological model, including  $\Omega_\Lambda$ ,  $\Omega_m$ ,  $\Omega_b$ , the Hubble parameter and the parameters that describe the primordial power spectrum of density fluctuations. These parameters determine the density of hydrogen per unit length, the conversion from Mpc to wavelength in a spectrum, and the spatial variations of the density. The second set of parameters are astrophysical, rather than primordial, and they determine the ionization and thermal state of the low density hydrogen. The IGM is highly photoionized by ultraviolet photons from early stars and AGN. The  $\tau_{\text{eff}}$

is then sensitive to the evolution of the intensity and spectrum of the UV background, or UVB. The energy input per photoionization, and the competition between photoheating and the cooling from the adiabatic expansion together give the temperature of the low density IGM, an output rather than an input parameter.

Over the last decade numerical hydrodynamic simulations of the IGM have steadily improved in accuracy. We can now make artificial QSO spectra directly from the full hydrodynamical simulations and measure the statistical properties of the Ly $\alpha$  forest absorption in those spectra. As expected, we find that the absorption in the artificial spectra depends on the complete set of cosmological and astrophysical parameters. In Tytler et al. (2004, T04b) and Jena et al. (2005, J05) we showed how we can choose sets of input parameters for simulations that give artificial spectra that are statistically equivalent to the largest and best samples of real spectra. We can now use the simulations to decode the IGM.

When we match simulations to real QSO spectra we obtain joint constraints on the full set of cosmological and astrophysical parameters that we input to the simulations. We do not obtain constraints on individual input parame-

\* E-mail: dkirkman@ucsd.edu

† Visiting Astronomer, W.M. Keck Observatory, which is a joint facility of the University of California, the California Institute of Technology, and NASA

ters, except when we fix all the many other parameters at values obtained from other observations.

We find that the statistical properties of the Ly $\alpha$  forest are highly sensitive to many of the input parameters (Tytler et al. 2004; Bolton et al. 2005; Jena et al. 2005). When we compare to calibrated real spectra, we can expect to obtain joint constraints on sets of parameters that are competitive with the best measurements from other types of observations. This motivates us to improve the accuracy of the measurement of the IGM.

We also find that the comparison between numerical simulations and real spectra of the Ly $\alpha$  forest provides the most accurate measurements of the intensity of the UVB (Rauch et al. 1997; Tytler et al. 2004; Jena et al. 2005; Bolton et al. 2005).

We have found that two statistics in particular provide a good summary of the Ly $\alpha$  forest. One is the effective optical depth  $\tau_{\text{eff}}$ , and the other some measure of the clumping and temperature of the gas, such as the line width distribution, or the power spectrum of the QSO flux. In T04 we measured  $\tau_{\text{eff}}$  to high precision over the redshift range  $1.6 < z < 2.2$ . The aim of this paper is to extend the redshift range over which we can make detailed comparisons between simulations and data by providing a calibrated and precise measurement of the H I Ly $\alpha$  forest opacity over the redshift range  $2.2 < z < 3.2$ .

### 1.1 Previous Work

There has been extensive previous work dedicated to measuring the total amount of absorption in the Ly $\alpha$  forest, summarized in part by T04b and Meiksin & White (2004) and the references therein. Many of these measurements appear to differ, but Meiksin & White (2004) showed that much, but not all, of the disagreement between some measurements was caused by differences in treating errors. T04b discuss other differences that remain.

Although we have had spectra of the Ly $\alpha$  forest since 1972, it is only recently that we have had simulations of the quality to match highly accurate measurements of the mean amount of absorption.

The mean absorption is hard to measure for three reasons discussed at length in T04b: the continuum level, metal lines and sample size.

To measure the amount of absorption we must first guess the continuum prior to the absorption. This is relatively easy at  $z \simeq 2$ , hard at  $z \simeq 3$  and very hard at  $z > 4$  where there is little if any unabsorbed continuum remaining in the Ly $\alpha$  forest. T04b dealt with the continuum level by making and fitting artificial spectra that looked similar to the real spectra. They saw and fitted the emission lines in the Ly $\alpha$  forest of each individual spectrum (Tytler et al. 2004). These lines vary a lot from QSO to QSO (Tytler et al. 2004; Suzuki et al. 2005). Using the artificial spectra we were able to show that their continuum level was accurate to approximately 0.3%, after correction, and averaging over the Ly $\alpha$  forest of 77 QSOs.

The simulations that we compare to the Ly $\alpha$  forest spectra typically lack the resolution and physics required to give realistic metal absorption lines and Ly $\alpha$  lines from regions with column densities  $\log N_{\text{HI}} > 17.2 \text{ cm}^{-2}$ . We then need a prescription for dealing with metal lines and strong Ly $\alpha$  lines

in the Ly $\alpha$  forest. Some measurements ignore these lines, while others subtract some or most of them. At  $z = 1.9$  T04b showed that the metal lines contributed 15% and strong Ly $\alpha$  lines 7% of the absorption in the Ly $\alpha$  forest. However, they each contributed about the same amount to the total variance of the absorption as did the Ly $\alpha$  absorption in the low density IGM.

The last requirement for an accurate measurement of the mean amount of absorption in the Ly $\alpha$  forest is a large sample, ideally at least tens of QSOs. It had long been noted that there is conspicuous variation in the amount of Ly $\alpha$  forest absorption from QSO to QSO (Carswell et al. 1982; Kim et al. 2001), and T04b showed that the amount of variation on scales of  $\Delta z = 0.1$  (121 Å in the observed frame) is consistent with large scale structure for a primordial spectrum of perturbations with slope  $n = 0.95$ , and present amplitude  $\sigma_8 = 0.9$ .

Following Oke & Korycansky (1982) we define  $DA(z) = 1 - \overline{F}(z)$ , where  $F(z)$  is the observed flux divided by the continuum level, and  $\overline{F}(z)$  is the mean over many spectra at a given redshift. T04b found that  $DA(z = 1.9) = 0.151 \pm 0.006$  including all absorption at rest frame wavelengths 1070 – 1170 Å towards 77 QSOs. The error here is partly from the continuum level, and partly from the sample size. T04b estimated the metal line absorption from wavelengths between the Ly $\alpha$  and C IV emission lines, from both their own spectra and from spectra of Sargent et al. (1988). They estimated the strong Ly $\alpha$  lines from the statistics of such lines in other spectra. When they subtracted both the metal lines and strong Ly $\alpha$  lines the DA drops to  $0.118 \pm 0.010$ . T04b estimated that approximately 5 ideal spectra, all at the same  $z_{\text{em}}$  with no continuum errors, and no metal lines or strong Ly $\alpha$  lines would give DA with an error of 0.01 at a single redshift,  $z = 1.9$ . High resolution spectra might approach this limit.

In Jena et al. (2005) we presented a set of 40 fully hydrodynamic simulations of the IGM at  $z = 2$ . We derived scaling laws that related the parameters of simulated spectra to the parameters that we input to the simulations. When we apply the scaling laws to a simulation, we can predict the output parameters to higher accuracy than the typical measurement error in real spectra. We were able to predict the most common line width ( $b$ -value) to  $0.3 \text{ km s}^{-1}$  and the  $\tau_{\text{eff}}$  to 0.0027, both approximately a factor of four smaller than the measurement errors in the real spectra. In this paper we address the need for improved measurements.

### 1.2 Our Approach

We apply the methods of T04b to make a calibrated measurement of DA at  $2.2 < z < 3.2$ . The basic idea is that we will ensure that our continuum fitting is unbiased by simultaneously fitting our real data and artificial spectra that have been carefully prepared to exhibit the types of errors shown in real spectra. The hope is that any systematic errors in our continuum fitting will manifest themselves in our continuum fits to both the real data and the artificial data. We can then measure them in the artificial data and apply the appropriate corrections to our real data.

We will generally follow the details of T04b, with some specific exceptions. Here we made artificial continuum and emission line spectra using principal component spectra,

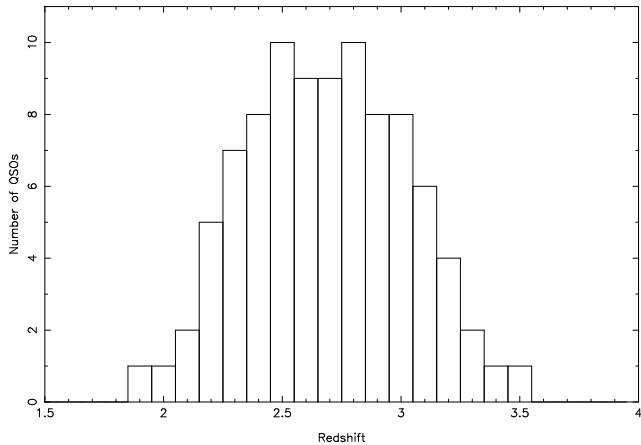


**Figure 1.** The number of H IRES QSOs which have complete Ly $\alpha$  forest coverage in different redshift bins

rather than real HST spectra (Suzuki et al. 2005). We made the Ly $\alpha$  forest absorption from randomly placed Voigt profiles with parameter distribution functions taken from the literature, instead of using a simplified model of the IGM to produce the Ly $\alpha$  forest absorption. In addition, we added metal and strong Ly $\alpha$  lines to the artificial spectra. However the main difference is that we now use H IRES spectra with 8 km s $^{-1}$  resolution in place of the 250 km s $^{-1}$  resolution spectra that we used in T04b. The higher resolution comes with many times more photons per  $\text{\AA}$  and allows us to place accurate continua at higher redshifts.

## 2 DATA SAMPLE

We use a collection of QSO spectra obtained with the H IRES spectrograph on the Keck telescope (Vogt et al. 1994). These spectra were collected between 1994 and 2004, for a variety of programs. The 24 QSOs that we use in this paper were selected from among our H IRES spectra for the following reasons: (1) they have significant coverage for Ly $\alpha$  lines with  $2.2 < z < 3.2$ , (2) they have SNR 8 – 70 per 2.1 km s $^{-1}$ , with a mean of 20 and (3) we were able to perform high quality flux calibration of the QSO spectra. The list of spectra we use in this paper is given in Table 1.

The spectra were all obtained with the original Tektronix 2048 x 2048 24 micron pixel CCD in H IRES up until August 2004. We used Tom Barlow’s makee package to extract the CCD images and apply the wavelength calibration. The individual exposures were flux calibrated and combined via the procedure described in Suzuki et al. (2003). We measured the redshift of each QSO from the estimated peak of the Ly $\alpha$  emission line, which is given in Table 1 as  $z_{\text{em}}$  (e.g.  $z_{\text{em}}$  is not the systemic redshift of the QSO).

A histogram of the number of different QSOs that contribute to each  $\Delta z = 0.1$  redshift bin is shown in Figure 1.

## 3 ARTIFICIAL SPECTRA

We attempted to make artificial spectra that mimic real spectra in every important way, including emission lines,

**Table 1.** H IRES Ly $\alpha$  forest spectra used to measure DA

Identifier	RA (B1950)	Dec (B1950)	$z_{\text{em}}$	V
q0014+8118	00 14 04.45	+81 18 28.6	3.366	16.50
q0042-2627	00 42 06.42	-26 27 45.3	3.289	18.47
q0100+1300	01 00 33.38	+13 00 12.1	2.681	16.57
q0105+1619	01 05 26.97	+16 19 50.1	2.640	16.90
q0119+1432	01 19 16.21	+14 32 43.2	2.870	16.70
q0130-4021	01 30 50.28	-40 21 51.0	3.023	17.02
q0139+0008	01 39 40.85	+00 08 17.8	3.405	18.32
q0301-0035	03 01 07.70	-00 35 03.0	3.231	17.62
q0322-3213	03 22 11.18	-32 13 34.6	3.302	17.95
q0450-1310	04 50 54.00	-13 10 39.0	2.300	16.50
q0449-1645	04 49 59.00	-16 45 09.0	2.677	17.00
q0741+4741	07 41 42.05	+47 41 53.4	3.210	17.50
q0930+2858	09 30 41.40	+28 58 53.0	3.428	17.50
q1005+3638	10 05 44.13	+36 38 02.4	3.125	17.85
q1155+2640	11 55 07.62	+26 40 37.0	2.850	17.60
q1200+1539	12 00 57.62	+15 39 36.1	2.981	17.10
q1208+1011	12 08 23.81	+10 11 08.5	3.822	17.90
q1243+3047	12 43 44.90	+30 47 54.0	2.560	17.00
q1244+3143	12 44 48.83	+31 43 02.9	2.961	17.90
q1320+3927	13 20 41.02	+39 27 46.8	2.985	17.06
q1337+2123	13 37 47.92	+21 23 54.1	2.700	17.90
q2223+2024	22 23 13.32	+20 24 58.5	3.560	18.38
q2337+1845	23 37 13.08	+18 45 12.2	2.620	17.00
q2344+1229	23 44 13.2	+12 28 50	2.784	17.5

cosmic ray hits, echelle blaze, and flux calibration errors. For each real spectrum, we made four artificial spectra with the same redshift and noise properties and various absorption lines.

We made the unabsorbed continuum shape, including emission lines with the principal component spectra described by Suzuki et al. (2005). The artificial spectra have a wide variety of shapes, and include realistic emission lines between Ly $\alpha$  and Ly $\beta$ . The exact shape and strength of the emission lines was different for each artificial spectrum.

We made the H I absorption from discrete lines, with the line distribution functions given in Kirkman & Tytler (1997). The artificial spectra used in this paper have lines of all column densities,  $10^{10} < N_{\text{HI}} < 10^{18}$  cm $^{-2}$ , and we placed lines at random redshifts, from the  $z_{\text{em}}$  listed in Table 1, down to zero redshift.

If a real spectrum had a DLA with  $\log N_{\text{HI}} > 10^{19.5}$  cm $^{-2}$ , we added a line with the same  $\log N_{\text{HI}}$  at the same wavelength to all the accompanying artificial spectra.

With each H I absorber, we also added the strong doublet absorption lines of C IV, Si IV, and Mg II to the artificial spectrum. We held the H I/X column density ratio constant for each metal ion, and the width of each metal absorber was calculated by assuming that the H I  $b$  values were entirely thermal. This resulted in an artificial metal forest that was superimposed on the H I forest, which made the artificial spectra look more realistic when inspected closely.

The artificial spectra used in this paper were generated differently than the spectra we used for the same purpose in T04b. The spectra in T04b were generated via a toy model of the IGM that mimicked the large scale structure, but we did not add metal lines of the Ly $\alpha$  lines of Lyman limit systems.

We added noise to the artificial spectrum, and at-

tempted to match the approximate SNR level of each real spectrum. We based the noise levels in our simulated spectra upon the estimated error estimates in the real echelle spectra. The resulting artificial spectra have SNR similar to their real spectra except for three of the five with  $\text{SNR} > 45$ , where the artificial have a SNR too low by approximately 1.5.

We also added a blaze effect to the artificial noise levels to simulate the increased SNR obtained at the center of each echelle order. Furthermore, we added small fluxing errors, by offsetting different echelle orders by the blaze function multiplied by a Gaussian random deviate with  $\sigma = 2\%$ , which is larger than the expected fluxing errors in the data (Suzuki et al. 2003). In Figure 2 we show an example of artificial spectra, below the real spectra they approximate.

Although we see differences between our artificial and real spectra, they do not concern us. Since we placed the Ly $\alpha$  lines at random redshifts, the artificial spectra lack large scale structure. The artificial spectra also show more total absorption than real spectra, generally about 5% more total absorption over the redshift range  $2.4 < z < 3.0$ . As we show in the next section, we are able to fit continua very well for a wide range of total absorption, so we do not believe that the minor differences between our real spectra and the artificial ones have significantly changed our results.

## 4 CONTINUUM FITTING

Four undergraduate authors, SH, KJ, CM, and GS, took a training program to fit QSO continua. They fit artificial QSO spectra that were not matched to any specific QSO. These spectra had a variety of emission redshifts, SNR, emission line profiles, and flux calibration errors. The four all fit the same spectra, and after they completed a few spectra, we revealed the true continuum level and we discussed their fit. Within a few weeks two of them were able to fit continua as well as any of us.

After this training completed, we asked them to fit the real and matched artificial spectra. We provided spectra in sets comprising one real spectrum and two artificial ones matched to that real one. Each fitter was given the same copy of the real spectrum, but different versions of the artificial spectra. We did not reveal which was the real spectrum in a set.

The results indicate that the two best fitters were excellent. The other two fitters were less accurate, and more importantly, occasionally had made large fitting errors. Thus for the measurement of DA, we used the average continuum of the two best fitters, and do not discuss the results of the other two fitters any further.

The standard deviation of the continuum fit errors per spectral segments of length  $\Delta z = 0.1$  is 1.2%. We fit a total of 96 artificial spectra, four per QSO (two per fitter per QSO), and there were a total of 275 segments of length  $\Delta z = 0.1$  in these artificial spectra. Averaged over all 275 segments, the continua of the two best fitters were above the true continua by 0.29%. If the fits were unbiased, and the errors per segment were uncorrelated we would expect the bias to be  $1.2/\sqrt{275} = 0.07\%$ . As in T04b we have measured a small bias.

In Figure 3 we show a weak correlation between the er-

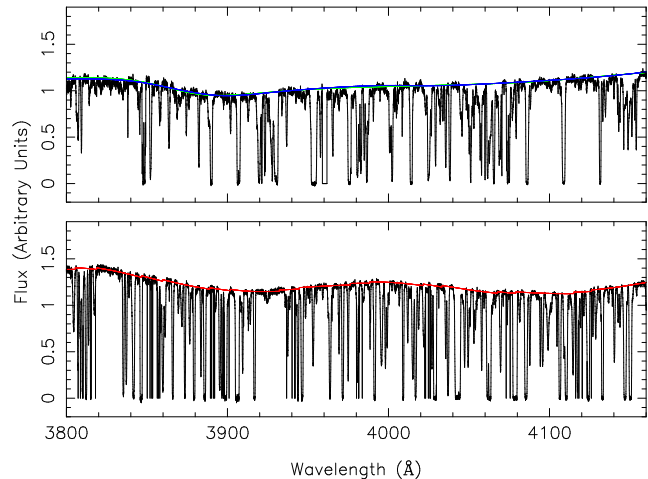


**Figure 2.** Example of our data, our continuum fits, and the artificial spectra we used to verify our continuum fitting ability. The top panel shows the spectrum of Q1243+3047 along with the individual continuum fits of our two best fitters. The bottom panel shows one of the four artificial spectra that we made similar to the Q1243+3047 spectrum. Q1243+3047 is representative of the spectra at the top end of the SNR distribution for spectra used in this paper. The lowest major tick mark is the zero flux level. We show rest wavelengths 1070 – 1170 Å.

ror in the continuum fit to the artificial spectra and the mean amount of absorption in a spectral segment of length  $\Delta z = 0.1$ . We fit this correlation as bias  $B = 0.0098 - 0.0249DA$  and we corrected all our real continua using this fit to remove the trend. After this correction when we average over all artificial spectra there is no remaining bias. All the data on the real HIRES spectra that we give in the paper have had this correction applied. We followed a similar procedure in T04b. After removing the bias associated with the mean flux of each spectral segment, we see no correlation between the error in the continuum fit to the artificial spectra and their SNR. We have not measured whether the bias varies from object to object, or as a function of  $z$ .

Based upon our ability to continuum fit artificial spectra, we conclude that errors in continuum placement are not a significant source of error when measuring DA in high resolution, moderate SNR spectra at  $z < 3.0$ .

## 5 MEASUREMENT OF THE MEAN FLUX

To avoid confusion between multiple Lyman series lines, we restrict our analysis to the region between the Ly $\alpha$  and Ly $\beta$  emission lines of each QSO. To avoid continuum fitting problems associated with rapidly changing emission line profiles, and possible contamination from the proximity effect, we further restrict our measurement of DA to the rest frame wavelengths 1070 – 1170 Å.

### 5.1 Removal of LLS absorption

Because many of our objects were originally observed as part of our program to measure the primordial deuterium abundance, which can only be measured in LLS (including DLAs), our data contains more LLS absorption than would a

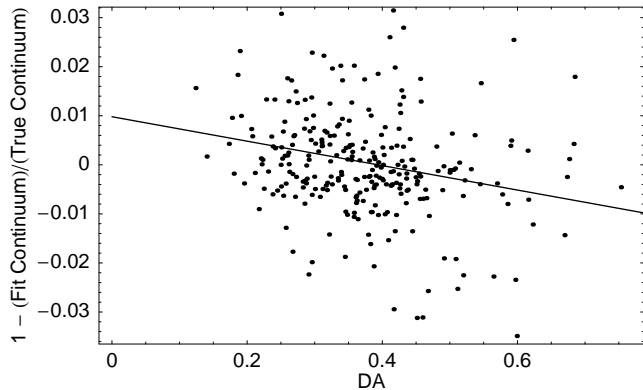


**Figure 3.** The difference between the fit continuum level and the true continuum level for each  $\Delta z = 0.1$  segment in the artificial spectra. We plot this difference against the mean DA in each spectral segment. There is a weak trend with the amount of absorption, which we fit with the solid line. There are more points on this plot than we have in our real data, because we fit four artificial spectra for each real spectrum in our analysis. Note that the magnitude of the effect is quite small.

completely random sample. This prevents us from removing the LLS absorption statistically, as we did in T04b. To overcome this problem, we have masked out all regions of each spectrum containing Ly $\alpha$  absorption associated with identified LLS. By mask, we mean that the pixels were marked as being unusable, and were not used in any further computations. In practice, our LLS identifications are probably not complete, but we believe that we identified and masked all absorbers with  $N_{\text{HI}} > 10^{19} \text{ cm}^{-2}$ .

If the QSO was originally observed as part of our primordial D/H program, we also masked out any metal lines that might be at the known redshift of the targeted LLS. All wavelengths within  $2000 \text{ km s}^{-1}$  of an H I, C IV, Si IV, C III, Si III, C II, or Si II transition at the D redshift were masked. The transitions were masked based solely on the redshift, the transition rest wavelength, and the fact that there is metal absorption associated with the system in which we had searched for D. No attempt was made to fit the metal absorption.

## 5.2 Removal of metal line absorption

We have not attempted to identify and mask individual metal lines in the Ly $\alpha$  forest. While many of the spectra used in this paper have enough SNR to identify some of the absorption in the Ly $\alpha$  forest, manual removal of metal absorption is likely to be very incomplete, and we will not know how much absorption was missed. Instead, we will use the method described in T04b, and subtract the metal absorption statistically. In this section we use the notation from T04b, summarized in Table 1 of that paper. Briefly, DM refers to the amount of absorption from metal lines alone, and DM4 refers to the DM from metal lines listed in Table 3 of SBS88 averaged into bins of size  $\Delta z = 0.1$ .

We have measured the amount of absorption from metal lines in spectra published for 52 QSOs in Sargent et al. (1988, SBS88). We previously did this in T04b §8.1 for 26 QSOs with  $1.7 < z_{\text{em}} < 2.3$ . We now add the remaining QSOs listed in SBS88, to cover  $1.7 < z_{\text{em}} < 3.54$ . We sum

the equivalent widths of all the metal lines listed for the 52 QSOs in Table 3 of SBS88 from rest wavelengths 1225 – 1500 Å. We group the lines in bins of length 121.567 Å in the observed frame, corresponding to  $\Delta z = 0.1$  for Ly $\alpha$ . In T04b we called these DM4 values. We now have 354 DM4 values, with a mean of  $0.0191 \pm 0.0017$  and  $\sigma(\text{DM4}) = 0.0312$ , both slightly larger than the values (mean  $0.0167 \pm 0.0022$ ,  $\sigma = 0.0274$ ) in T04b. The mean observed wavelength is now 4764.4 Å, compared to 4124.8 Å in T04b.

We attempted to remove all absorption lines from systems that appeared to be associated with the QSOs. These systems produce large BAL like lines that are concentrated in certain emission lines, including Si IV, N V and O VI. The Si IV and especially the N V lines can contribute a lot to the DM estimate. However, the lines of these associated systems will have little effect on the total metal absorption in the DA region because O VI is excluded. We found six QSOs with conspicuous strong associated N V absorption that was responsible for many of the largest DM measurements of any segments in the sample. We also removed all lines from systems with  $\beta = v/c < 0.01$ , corresponding to velocities within  $3000 \text{ km s}^{-1}$  of the QSO. This value is large enough to remove most associated systems, without removing too many intervening systems. This criterion removed Si IV from 6 additional QSOs, and a few C II and Si II lines. We also removed the occasional Galactic Ca II at zero redshift. After removing these absorption lines, the mean DM decreased 18% to  $0.0157 \pm 0.0013$  and the standard deviation decreased 21% to  $\sigma(\text{DM4}) = 0.0248$ .

Following T04b, we re-fit the DM4 values as a function of wavelength in the rest frame of the QSO  $\lambda_r$  and observed wavelength  $\lambda_o$

$$\text{DM5}(\lambda_r) = 0.01564 - 4.646 \times 10^{-5}(\lambda_r - 1360), \quad (1)$$

and

$$\text{DM6}(\lambda_o) = 0.01686 - 1.798 \times 10^{-6}(\lambda_o - 4158). \quad (2)$$

(The slope of  $\text{DM6}(\lambda_o)$  was erroneously listed as  $7.136 \times 10^{-5}\%$  in T04b Eqn. 13, it should be  $7.136 \times 10^{-4}\%$ ). These fits supersede those given in T04b, both because the sample is twice as large, and because we did not remove associated systems in T04b. Note that here we give the DM as absolute values, while in T04b we gave the DM values in percentages.

The removal of the associated systems has no significant effect on the intercepts, but a large effect on the slopes, because the N V lines concentrate near the minimum  $\lambda_r$  that we used from SBS88. Removing the associated systems without enlarging the sample causes a slight decrease in the slope with  $\lambda_r$  while increasing the sample has no additional effect. For  $\lambda_o$  half the decrease in the slope comes from the removal of the associated systems and the other half from the enlargement of the sample.

We want DM as a function of both  $\lambda_o$  and  $\lambda_r$ . We see a clear trend of DM increasing as  $\lambda_r$  decreases, but no significant trend with  $\lambda_o$ , and hence no strong evolution with  $z_{\text{em}}$  and  $z_{\text{abs}}$ . The tendency for DM to rise with falling  $\lambda_r$  is hard to see in plots, but appears to come from a smaller fraction of segments with no absorption lines at lower  $\lambda_r$ .

We choose to correct each bin, from Kast and HIRES, by the DM for its  $\lambda_o$  assuming it is at  $\lambda_r = 1120 \text{ Å}$ . The DM values range from  $\text{DM}(1070) = 0.0291$ , to  $\text{DM}(1120) = 0.0268$  in the center of our  $\lambda_r$  range, to  $\text{DM}(1170) = 0.0245$ .

In T04b we used  $DM3 = 0.023 \pm 0.005$  for all segments. We now use  $DM(1120) = 0.0268$ , for all segments, and we simultaneously correct for the slight trend with  $\lambda_o$  given by Eqn. 2. At the mean  $\lambda_o$  of the Kast sample we measure  $DM(3525) = 0.01799$  while for the HIRES sample  $DM(4498) = 0.01624$ , both at the mean  $\lambda_r$  of the SBS88 sample:  $1357.2 \text{ \AA}$ . We apply the  $\lambda_o$  correction by multiplying by  $\tau_{\text{eff}}(\lambda_o)/\tau_{\text{eff}}(4764.4 \text{ \AA})$ , where  $4764.4 \text{ \AA}$  is the mean  $\lambda_o$  of the SBS88 sample. For example, we calculate  $\tau_{\text{eff}}$  at  $4498 \text{ \AA}$ , to be  $1.03 \times 0.02715$  corresponding to  $DM = 0.0276$ . As we explained in Jena et al. (2005), we subtract the  $\tau_{\text{eff}}$  values corresponding to the DM from the  $\tau_{\text{eff}}$  corresponding to the DA. We do not directly subtract  $DA - DM$ .

Since the DM values that we use are now larger than in T04b, the DA values are smaller, and the changes are most at the lowest  $z_{\text{abs}}$ .

Although we have improved upon T04b, we do not have a definitive measurement of DM. Three issues remain. First, we extrapolate in  $\lambda_r$  well beyond the limit of the data. Second, we use all the metal lines listed in SBS88, without regard for the equivalent width. Their SNR was approximately constant with wavelength in the relevant wavelength range, other than an increase in the N V emission line. Since their spectra do not have the resolution or SNR to see weak lines, the DM values we obtain from their spectra will be too small, and our DA too large. Third, our masking the lines of LLS may leave too few metal lines compared to the DM from SBS88. This error would make our DA too small. We masked all the metals from one LLS in most QSOs. These QSOs were selected because they contained these LLS, and hence we expect that they would have excess metals if we did not apply this mask. However, some of a random sample of QSOs would have LLS by chance, and hence we may have over corrected. This error will tend to cancel that from the numerous weak metal lines missed from the SBS88 line lists.

As a sanity check, we measured the amount of (unmasked) metal absorption in the six of our spectra that have significant coverage redward of the Ly $\alpha$  emission line. In those six spectra we measured the mean metal absorption over the observed wavelengths that correspond to the Ly $\alpha$  forest between  $2.2 < z < 3.2$  to be 2.1%. This value likely has large errors associated with it because it has been measured from only six QSOs, but it does increase our confidence the our general metal line removal based on the results of SBS88 is not wildly inaccurate.

### 5.3 Measurement of mean DA in $\Delta z = 0.1$ spectral segments

After masking targeted Deuterium systems and LLS with obvious Ly $\alpha$  lines, we measured the mean flux in spectral segments of  $\Delta z = 0.1$ . We started at a rest wavelength of  $1070 \text{ \AA}$  (or the lowest wavelength with data in cases of incomplete spectral coverage) in each QSO, and computed the mean flux of all segments that are fully contained between the rest wavelengths of  $1070$  and  $1170 \text{ \AA}$ . There are typically three  $\Delta z = 0.1$  segments in an individual QSO spectrum. We discard incomplete segments and any segment with more than 10% of it's flux masked for any reason, e.g. a DLA in a spectrum will cause at least one, and frequently two segments in a given QSO spectrum to be discarded. Finally,

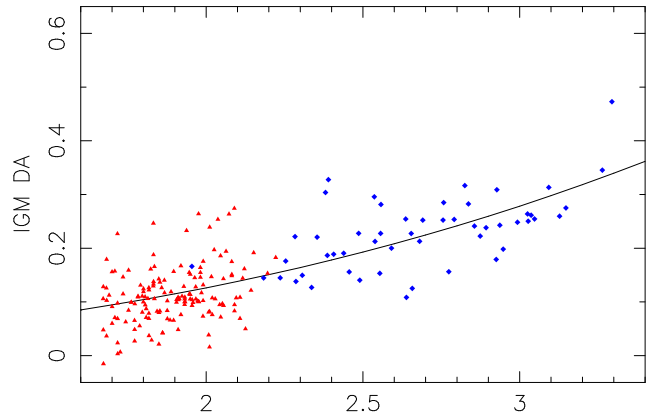


**Figure 4.** DA as a function of redshift. Each point shows the DA measured along a particular line of sight over a path of length  $\Delta z = 0.1$ . The light triangles are the data from 77 QSOs used by T04b (observed total absorption, minus mean absorption by Ly $\alpha$  of LLS and metals), while the dark diamonds show the new data from 24 QSOs from this paper (excluding individual Ly $\alpha$  of LLS, and minus the mean metal absorption). This plot does not show part of the data at the higher redshift end of each spectrum because we do not show bins that are partly sampled by a spectrum.

we subtracted the anticipated metal absorption from each segment, as described in §5.2.

Our results are shown in Figure 4, where we also show the results for the Kast spectra from T04b. Figure 4 shows only the absorption of the low column density Ly $\alpha$  forest – we have attempted to remove the Ly $\alpha$  of all LLS and all metal line absorption for all the Kast and HIRES spectra. For both the HIRES and Kast spectra we subtracted the same mean amount of metal absorption from each Kast point. For the Ly $\alpha$  of the LLS we subtracted the mean for all the Kast points, but we masked individual Ly $\alpha$  lines for the HIRES points.

### 5.4 DA as a function of redshift

To tabulate the mean DA as a function of redshift, we binned the data shown in Figure 4 into redshift bins of width  $\Delta z = 0.2$ . We estimated the mean DA of each bin to be simply the mean value of the points in the bin. We estimated the error to be the standard deviation of *all* the points (see §5.5, we compute the standard deviation from the best power law fit to the data) divided by the square root of the number of points in each bin. Using the standard deviation of all points instead of the standard deviation of just the points in each bin gives nearly identical results for bins with large numbers of points, but seems to be much better behaved for bins with small numbers of points. Our results are in Table 2 and shown in Figure 5.

DA as a function of  $z$  is well fit by a power law of the form  $A(1+z)^\gamma$ . Minimizing  $\chi^2$  to the points in Table 2 gives  $A = 0.0062$  and  $\gamma = 2.75$ . The  $\chi^2$  of the best fit is 8.69 and the reduced  $\chi^2$  for 7 degrees of freedom (9 data points - 2 parameters) is 1.24.

The dashed lines in Figure 4 enclose the  $\pm 1\sigma$  confidence interval fits. They are produced by taking the envelope that contains all power law fits with  $\chi^2 < \chi^2_{\text{min}} + 2.3$ . Thus the

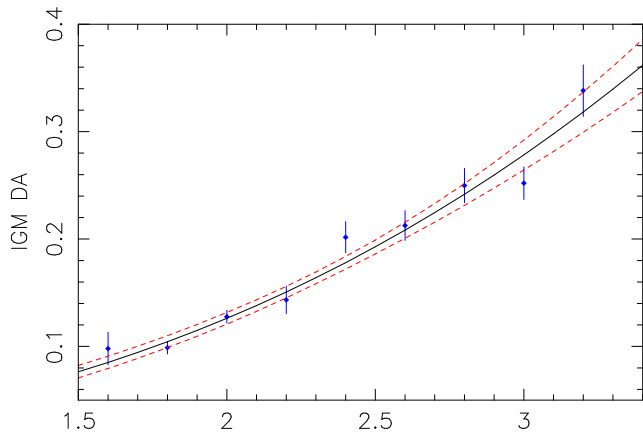


**Figure 5.** DA as a function of redshift. Here we have binned the data points shown in Figure 4 into bins of  $\Delta z = 0.2$ . The solid line shows the minimum  $\chi^2$  fit of the function  $A(1+z)^\gamma$ . We find  $A = 0.0062$  and  $\gamma = 2.75$  give  $\chi^2 = 8.69$  for seven degrees of freedom. The dashed lines show the  $\pm 1\sigma$  confidence interval on the fit.

**Table 2.** Measured IGM DA values in  $\Delta z = 0.2$  redshift bins

$z$ center	DA	$\sigma_{\text{DA}}$	Fit DA	Fit $\sigma_{\text{DA}}$
1.6	0.098	0.015	0.0851	0.0057
1.8	0.099	0.006	0.1044	0.0055
2.0	0.128	0.006	0.1262	0.0055
2.2	0.143	0.013	0.1507	0.0054
2.4	0.202	0.014	0.1780	0.0059
2.6	0.213	0.014	0.2083	0.0074
2.8	0.250	0.016	0.2417	0.0101
3.0	0.252	0.015	0.2783	0.0139
3.2	0.338	0.024	0.3183	0.0187

plotted error bounds are not power laws, but each point on the error curves corresponds to a point on a power law that fits our data. The last column in Table 2 gives the difference between the bounds divided by two.

We do not give errors for  $A$  or for  $\gamma$ . The  $A - \gamma$   $\chi^2$  manifold is complex, and it is not well approximated by only two numbers ( $\sigma$  for  $A$  and  $\gamma$ ). Attempts to do so in the past (Steidel & Sargent 1987; Press et al. 1993; Kim et al. 2001), have lead to all sorts of confusion in the literature – consider the efforts of Seljak et al. (2003) and Meiksin & White (2004) to determine the allowed values of  $\tau_{\text{eff}}$  at various redshifts. We recommend use of the results given in Table 2.

Note that the small dip in DA that we observed at  $z > 2.2$  in Fig. 22 of T04b is not present in the new HIRES data. The combined HIRES + KAST data seems to be well fit by a single power law, and no significant deviations from a power law are present in our data.

### 5.5 Dispersion of DA in $\Delta z = 0.1$ spectral segments

The new points from this work show less dispersion than the points in T04b. This is consistent with the fact that we have removed LLS absorption before calculating the mean flux in each point, while T04b calculated the mean flux in

each point with the LLS present, and then subtracted the LLS absorption statistically. While both results will give the same mean value for the H I Ly $\alpha$  forest opacity, the T04b method will include the substantial dispersion of the LLS absorption.

The standard deviation of the HIRES DA points (each covering  $\Delta z = 0.1$ ) about the mean given by the power law fit is  $\sigma_{\text{DA}} = 5.2^{+0.6}_{-0.4}$  % over redshifts  $2.2 < z < 3.2$ . This  $\sigma_{\text{DA}}$  value includes the intrinsic variance of the Ly $\alpha$  forest, the variance of metal line absorption (we removed the mean, not the individual metal absorption), and the variance of our continuum fitting errors. It should not include a significant contribution from LLS absorption, since we masked the Ly $\alpha$  absorption associated with LLS before measuring any DA values.

We can subtract variances (squares of standard deviations) to estimate the standard deviation of the absorption by Ly $\alpha$  from the low density IGM alone. As in T04 §9, we work with mean values in segments of length  $\Delta z = 0.1$ . We now repeat the calculations given in T04, considering only the HIRES spectra. We take the standard deviation of the metal absorption as 3.7 %, where we have scaled the value 3.1 % in Table 4 of T04b by the mean metal absorption which is now DM = 2.76 %, up from 2.3 %. We also use the standard deviation of the continuum fitting errors 1.2 % (§4). We find that the intrinsic variation of the mean amount of absorption in the Ly $\alpha$  forest over  $\Delta z = 0.1$  segments is  $\sigma(\Delta z = 0.1) = 3.4^{+1.0}_{-1.2}$  %. This value is a mean from the whole  $z$  range, centered near  $z = 2.7$ . At  $z = 2.7$  the mean total DA per segment, including metals but not Ly $\alpha$  lines of LLS, is 0.246, and after subtracting the metals it drops to 0.2246.

The  $\sigma(\Delta z = 0.1)$  value from HIRES spectra agrees with the value that we calculated in T04b (section 9.4) for Kast spectra:  $\sigma(\Delta z = 0.1) = 3.9^{+0.5}_{-0.7}$  % at  $z = 1.9$ . The error is larger now, because we have fewer DA measurements giving a larger error on the measurement of the standard deviation of the DA values. We expect that  $\sigma(\Delta z = 0.1)$  will increase with increasing  $z$  because the power spectrum of the flux in the Ly $\alpha$  forest increases with increasing redshift (Croft et al. 2002; McDonald et al. 2004). We do not see this, but this may be because our measurement errors are large and not well determined. In T04b we did not subtract the continuum fitting error because it appeared to be small, and was not well determined. We found contradictory evidence that the continuum fit error might be large, in which case the  $\sigma(\Delta z = 0.1)$  value should be less than the  $3.9^{+0.5}_{-0.7}$  %.

We conclude that 24 QSOs is adequate to get the mean DA, but we would prefer far more QSOs to obtain an accurate measurement of the variance in the DA.

## 6 DISCUSSION

Our DA results are in general agreement with the values of the literature summary given in Meiksin & White (2004, Table B1). However, we find approximately 0.03 less absorption at all redshifts. This is consistent with the fact that we have attempted to measure only the absorption due to the Ly $\alpha$  forest, while Meiksin & White (2004) gave values for all absorption in the Ly $\alpha$  forest region of a spectrum.

At  $z = 2.2$ , our results are also consistent with

Schaye et al. (2003), who also attempted to measure only the absorption associated with the Ly $\alpha$  forest. They only removed metals absorption they could identify directly in the absorption spectra, so their removal completeness is unknown, and is probably a function of redshift. However, we find a shallower redshift evolution and less absorption at  $z = 3.0$ .

The best fit value of  $DA = 0.278$  at  $z = 3.0$  is lower than we expected to find when we started this work. In T04b and J05 we developed a concordance model of the Ly $\alpha$  forest at  $z = 1.9$  – this model is referred to as model “A” in T04b and J05. Model A uses a uniform UVB with the shape and redshift evolution due to Haardt & Madau (2001), and displayed graphically in Paschos & Norman (2005). Model A, while giving the measured value of  $DA$  at  $z = 1.9$ , predicts  $DA = 0.34$  at  $z = 3$ . The clear implication is that there are more ionizing photons at  $z = 3$  than predicted by Haardt & Madau (2001). J05 showed that the naive expectation that  $\tau_{\text{eff}}$  scales like the H I ionization rate is valid at  $z = 2$ . Assuming that this result holds at  $z = 3$ , and translating  $DA$  into  $\tau_{\text{eff}}$ , we find an H I ionization rate of  $\Gamma_{-12} = 1.3 \pm 0.1$ , or 1.3 times the value predicted by Haardt & Madau (2001). The error comes from propagating the observed error on  $DA$  through the J05 scaling relation. The real error is likely to be larger, because there is some disagreement as to the scaling relationship between  $\Gamma$  and  $\tau_{\text{eff}}$ . While J05 found  $\Gamma \propto \tau_{\text{eff}}^{-1}$ , Bolton et al. (2005) found  $\Gamma \propto \tau_{\text{eff}}^{-1.44}$  at  $z = 2$ . Bolton et al. (2005) also found some change in redshift, with  $\Gamma \propto \tau_{\text{eff}}^{-1.61}$  at  $z = 3$ . If we use the Bolton et al. (2005)  $z = 3$  relationship instead of the J05 scaling relation, we instead find  $\Gamma_{-12} = 1.5$ .

Irrespective of the precise value of  $\Gamma$ , this data seems to indicate that it is larger than expected. It will be interesting to try to find the source of these extra photons.

## ACKNOWLEDGMENTS

All of the spectra used in this paper were obtained with the HIRES spectrograph, we would like to thank those who designed, built and maintain this amazing resource. We are grateful to the staff and observing assistants at the W.M. Keck Observatory, who have supported our observing for many years. The W.M. Keck Observatory is a joint facility of the University of California, the California Institute of Technology, and NASA. We are grateful to the referee, James Bolton, for several insightful comments. We thank Tom Barlow, who’s makee package was used to extract all of the HIRES spectra used in this project. Former UCSD students Xiao-Ming Fan, Scott Burles, Ed Lever, and John O’Meara helped to obtain some of the spectra used in this paper. SH was funded by the NSF REU program grant to the physics Dept. at UCSD. This work was funded in part by NSF grants AST-9900842 AST-9803137 and AST-0098731, and NASA grants NAG5-13113 and STScI grant HST-AR-10288.01-A.

## REFERENCES

- Carswell R. F., Whelan J. A. J., Smith M. G., Boksenberg A., Tytler D., 1982, MNRAS, 198, 91
- Croft R. A. C., Weinberg D. H., Bolte M., Burles S., Hernquist L., Katz N., Kirkman D., Tytler D., 2002, ApJ, 581, 20
- Haardt F., Madau P., 2001, in Clusters of galaxies and the high redshift universe observed in X-rays, Recent results of XMM-Newton and Chandra, XXXVIth Rencontres de Moriond, XXIst Moriond Astrophysics Meeting, March 10-17, 2001, Savoie France. Edited by D.M. Neumann & J.T.T. Van Modelling the UV/X-ray cosmic background with CUBA
- Jena T., Norman M. L., Tytler D., Kirkman D., Suzuki N., Chapman A., Melis C., So G., O’Shea B. W., Lin W., Lubin D., Paschos P., Reimers D., Janknecht E., Fechner C., 2005, MNRASsubmitted, astro-ph/0412557
- Kim T.-S., Cristiani S., D’Odorico S., 2001, A&A, 373, 757
- Kirkman D., Tytler D., 1997, ApJ, 484, 672
- McDonald P., Seljak U., Burles S., Schlegel D. J., Weinberg D. H., Shih D., Schaye J., Schneider D. P., Brinkmann J., Brunner R. J., Fukugita M., 2004, ApJsubmitted, astro-ph/0405013
- Meiksin A., White M., 2004, MNRAS, eprint arXiv:astro-ph/0205387, 350, 1107
- Oke J. B., Korycansky D. G., 1982, ApJ, 255, 11
- Paschos P., Norman M. L., 2005, ApJ (submitted, astro-ph/0412244)
- Press W. H., Rybicki G. B., Schneider D. P., 1993, ApJ, 414, 64
- Rauch M., Miralda-Escude J., Sargent W. L. W., Barlow T. A., Weinberg D. H., Hernquist L., Katz N., Cen R., Ostriker J. P., 1997, ApJ, 489, 7
- Sargent W. L. W., Boksenberg A., Steidel C. C., 1988, ApJS, 68, 539
- Schaye J., Aguirre A., Kim T.-S., Theuns T., Rauch M., Sargent W. L. W., 2003, ApJ, 596, 768
- Seljak U., McDonald P., Makarov A., 2003, MNRAS, 342, L79
- Steidel C. C., Sargent W. L. W., 1987, ApJ, 313, 171
- Suzuki N., Tytler D., Kirkman D., O’Meara J. M., Lubin D., 2003, PASP, 115, 1050
- Suzuki N., Tytler D., Kirkman D., O’Meara J. M., Lubin D., 2005, ApJ, 618, 592
- Tytler D., Kirkman D., O’Meara J., Suzuki N., Orin A., Lubin D., Paschos P., Jena T., Lin W.-C., Norman M., 2004, ApJ, astro-ph/0403688, 617, 1
- Tytler D., O’Meara J. M., Suzuki N., Kirkman D., Lubin D., Orin A., 2004, AJ, 128, 1058
- Vogt S. S., Allen S. L., Bigelow B. C., Bresee L., Brown B., Cantrall T., Conrad A., Couture M. *et al.*, 1994, in Proc. SPIE Instrumentation in Astronomy VIII, David L. Crawford; Eric R. Craine; Eds., Volume 2198, p. 362 Vol. 2198, HIRES: the high-resolution echelle spectrometer on the Keck 10-m Telescope. p. 362